Journal of Medicinal Chemistry

pubs.acs.org/jmc

Article

Discovery of Novel Anti-Breast-Cancer Inhibitors by Synergistically Antagonizing Microtubule Polymerization and Aryl Hydrocarbon Receptor Expression

Kun Wang,[§] Hui Zhong,[§] Na Li, Nairong Yu, Yujin Wang, Li Chen,* and Jianbo Sun*

Cite This: https://doi.org/10.1021/acs.jmedchem.1c01099

Read Online

ACCESS | Metrics & More | Article Recommendations | Supporting Information

ABSTRACT: A series of unreported dual-receptor inhibitors targeting both the tubulin colchicine site and AhR were designed and synthesized, and their anti-breast-cancer activities were evaluated. Compound **12** showed the strongest activity with an IC_{50} of 0.9 nM in MCF-7 cell lines. Besides, **12** could significantly inhibit cancer growth in MCF-7 xenograft tumor models with no obvious toxic effects and was more effective than the positive control (combretastatin A-4). With the in-depth study, it was found that **12** could induce apoptosis in breast cancer cells by making arrest in G2/M phase, depolarizing mitochondria and inducing intracellular reactive oxygen generation. This evident anticancer effect and the ability to inhibit cell migration were attributed to the synergistic antagonism of 12 on tubulin and AhR. In general, **12** was worthy of further research as an effective and safe anti-breast-cancer drug.

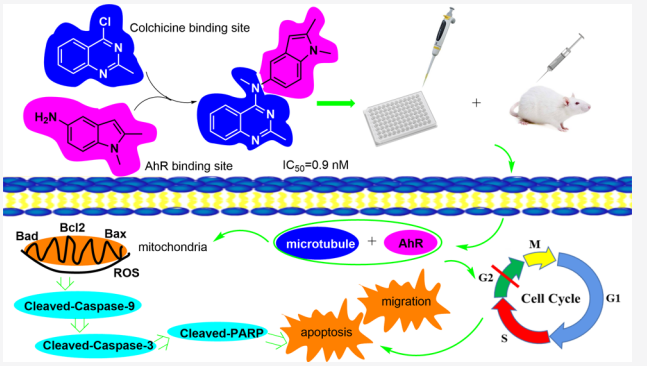

1. INTRODUCTION

Breast cancer is the most prevalent cancer in females, accounting for 30% of new cancer cases, making it the second leading cause of cancer deaths in female patients.[1] The recurrence and metastasis of breast cancer are important factors affecting the prognosis of breast cancer patients.[2] Consequently, it is imminent to find safe and effective therapeutic drugs to fight breast cancer, which is easy to metastasize and invade and difficult to cure. The development of new antimitotic drugs is currently an effective chemotherapeutic strategy in the treatment of breast cancer.[3] Since tubulin is the key structure of mitotic spindles, disruption of tubulin dynamics by antimitotic drugs can arrest cell division, thereby preventing cancer proliferation.[4] Antitubulin therapy has shown substantial therapeutic effects in clinical practice. However, since tubulin is widely present in cancer cells and normal cells, microtubule inhibitors have obvious toxicity in normal tissues. Additionally, patients' response rates are different and unpredictable, possibly due to cancer metastasis.[5]

Cancer metastasis is closely associated with the tumor microenvironment and is the cause of cancer death.[6] Evidence has shown that the aryl hydrocarbon receptor (AhR) is involved in the control of breast cancer metastasis and proliferation.[7,8] Furthermore, AhR was reported to activate members of the cytochrome P450 (CYP450) family, with CYP1A1 being crucial for regulating breast cancer cell proliferation and metastasis.[8,9] Nowadays, the development of the AhR/CYP1A1 signaling pathway inhibitors has become an innovative approach in breast cancer prevention and therapy.[10,11] Thus, based on the tubulin colchicine site and the ligand characteristics of AhR, we used the fragment-based design strategy to hybrid the scaffolds targeting the colchicine site with the fragment that can target the AhR binding site to develop duo-targeted inhibitors so as to inhibit the malignant proliferation and metastasis of breast cancer cells.

With effective binding capacity at colchicine sites, quinoline and quinazoline scaffolds are generally used as privileged structures to design antimitotic agents and tubulin polymerization inhibitors.[12−15] As reported, many of the AhR inhibitors involved privileged structures with a strong binding affinity, including indole and other aromatic nuclei, such as GNF351, PDM2, and StemRegenin 1.[16,17] Therefore, we hybridized quinazoline/quinoline scaffolds with indoles/aromatic nucleus and with aminomethyl as the linker to design and synthesize a series of dual-receptor inhibitors targeting both the tubulin colchicine site and AhR (Figure 1). The structure−activity relationship was investigated by modifying the indole/aromatic nucleus. According to the results of molecular docking, it could be inferred that the

Received: June 18, 2021

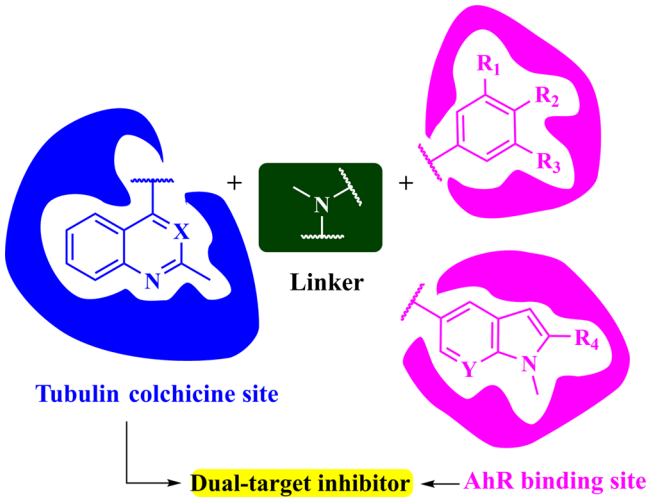

Figure 1. Design strategy of target compounds.

inhibitors we designed could effectively bind to the colchicine site. In this paper, the synthesis of target compounds, the evaluation of their antitumor activities, and the clarification of the antitumor mechanism for the most potential compound **12** have been reported.

2. RESULTS AND DISCUSSION

2.1. Chemical Synthesis. The synthetic sequence of dual-receptor inhibitors has been described in Scheme 1. The designed target products were obtained from 2-methyl-4-chloroquinoline and 2-methyl-4-chloroquinazoline. First, 2-methyl-4-chloroquinoline/2-methyl-4-chloroquinazoline and aniline/indoleamine derivatives were mixed in the presence of concentrated sulfuric acid to obtain the intermediates. Subsequently, the target compounds were obtained from the intermediates in the presence of sodium hydrogen and iodomethane.

2.2. Biological Assessment. *2.2.1. In Vitro Antiproliferative Activity.* To preliminarily determine the anti-breast-cancer activity *in vitro*, the IC_{50} value of all target compounds against MCF-7 cells was tested with microtubules overexpressed by the MTT assay. As a tubulin inhibitor, combretastatin A-4 (CA-4) was included as a comparative reference 18. As shown in Table 1, the influence of the substituents on the benzene ring for the activity was as follows: 4-*N*,*N*-diethylamino > 4-*N*,*N*-dimethylamino > 3,4-OCH_2O > 3,4-OCH_3 > CH_3 > benzene > 3,4,5-OCH_3/CF_3. These results showed that the electron-rich substituents contributed to the increase of the antiproliferative activity, while the activity decreased with the increase of electron-withdrawing groups. Besides, when the benzene ring was replaced by indole, the antiproliferative activities increased greatly, as the IC_{50} values (MCF-7 cells) of compounds **9**, **10**, **11**, and **12** were less than 4.5 nM and all better than CA-4 (IC_{50} = 4.8 nM). Moreover, the activities were further improved by replacing the 3-bit carbon atom of the quinoline ring with a nitrogen atom. Furthermore, compound **12** (IC_{50} = 0.9 nM) showed inhibitory activity on breast cancer cells greater than **11** (IC_{50} = 2.1 nM) as the 2-bit hydrogen on the indole ring was replaced by methyl groups.

Human breast cancer adriamycin-resistant cells (MCF-7/ADR) and two human normal cell lines including human normal hepatocyte cells (L-O2) and human normal mammary cells (MCF-10A) were chosen to further evaluate the reversal of drug resistance and cytotoxicities of target compounds. The cytotoxicities of most tested compounds in MCF-7/ADR were at the nanomolar level (from 0.9 to 912 nM) and were weaker in human normal cells than those in cancer cells.

2.2.2. Effects on Microtubule Networks of MCF-7 Cells. To elucidate whether such dual-receptor inhibitors targeted the microtubule, compound **12** was evaluated for its effect on microtubule networks of MCF-7 cells. Colchicine, an effective microtubule-destabilizing agent, was used as the control. As exhibited in Figure 2, the tubulin networks in negative control cells were normally arranged with plentiful and fibrous tubulins surrounded by the cell nuclei. However, when treated with **12** and colchicine, the microtubule tissues in the cells were severely contracted, indicating that the microtubule tissues were damaged. With the increase in concentration, the damage degree of microtubule tissues in MCF-7 cells also gradually increased. Specifically, microtubules were less affected at 0.5 nM and the network structure was clear, with the effect of colchicine produced being the same as 200 nM. When the concentration reached 4 nM, only sporadic microtubule tissues were found around the nucleus, indicating that **12** induced

Scheme 1. Reagents and Conditions: (a) Aniline/Indoleamine Derivatives, Concentrated Sulfuric Acid, Isopropanol, Reflux, 4 h; (b) Sodium Hydride, Iodomethane, Dimethyl Formamide, rt, 12 h

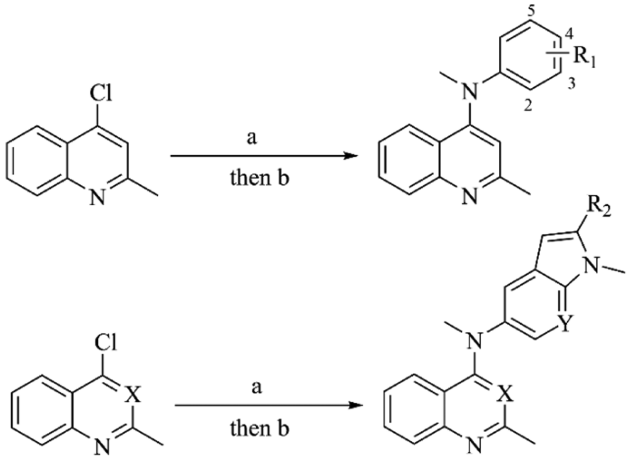

1 R_1=3,4,5-OCH_3
2 R_1=3,4-OCH_3
3 R_1=4-CH_3
4 R_1=3,4-OCH_2O
5 R_1=4-CF_3
6 R_1=4-benzene
7 R_1=4-N,N-Dimethylamino
8 R_1=4-N,N-Diethylamino

9 R_2=H, X=C, Y=N
10 R_2=CH_3, X=C, Y=C
11 R_2=H, X=N, Y=N
12 R_2=CH_3, X=N, Y=C

https://doi.org/10.1021/acs.jmedchem.1c01099
J. Med. Chem. XXXX, XXX, XXX−XXX

Table 1. Inhibitory Effects of Target Products on Cancer and Normal Cell Lines

	IC_{50} (μM)[a]			
compounds	MCF-7	MCF-7/ADR	MCF-10A	L-O2
1	>1	0.912 ± 0.036	>1	4.121 ± 0.816
2	0.097 ± 0.004	0.029 ± 0.001	0.473 ± 0.011	2.172 ± 0.680
3	0.103 ± 0.019	0.054 ± 0.003	0.184 ± 0.023	1.527 ± 0.196
4	0.054 ± 0.001	0.046 ± 0.001	0.127 ± 0.021	2.497 ± 0.120
5	>1	0.859 ± 0.031	>1	3.839 ± 0.698
6	>1	0.817 ± 0.020	>1	3.447 ± 0.749
7	0.943 ± 0.046	0.033 ± 0.001	0.049 ± 0.001	0.227 ± 0.019
8	0.025 ± 0.009	0.267 ± 0.020	0.012 ± 0.001	0.031 ± 0.001
9	0.0045 ± 0.0003	0.0061 ± 0.001	0.024 ± 0.001	0.010 ± 0.007
10	0.0024 ± 0.0001	0.0022 ± 0.0001	0.010 ± 0.001	0.0073 ± 0.0005
11	0.0021 ± 0.0002	0.0021 ± 0.0001	0.016 ± 0.001	0.0073 ± 0.0006
12	0.0009 ± 0.00006	0.0009 ± 0.00001	0.0093 ± 0.0008	0.0046 ± 0.0001
CA-4	0.0048 ± 0.0002	0.0031 ± 0.0001	0.099 ± 0.003	0.0103 ± 0.0004

[a]Values are expressed as mean ± SD of each compound from three independent experiments.

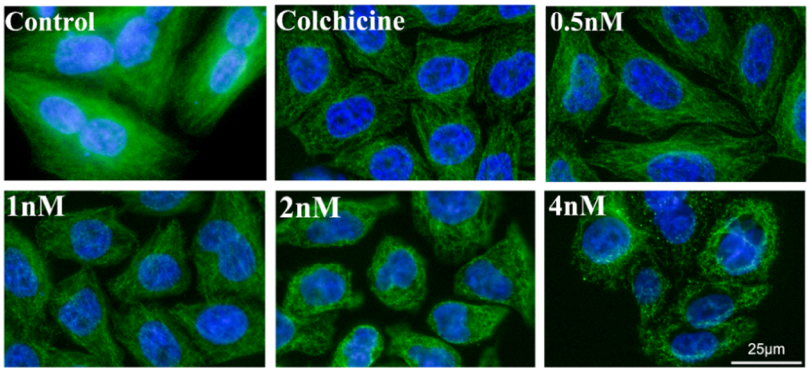

Figure 2. Effects of **12** on the cellular tubulin system intuitively observed by immunofluorescence.

destructions of the inner microtubule, which might ultimately cause apoptosis.

2.2.3. Evaluation of Tubulin Polymerization In Vitro. **12** was then evaluated for its effect on microtubule dynamics in MCF-7 cells. Paclitaxel and CA-4 were used as controls. As exhibited in Figure 3, paclitaxel showed a significant effect of

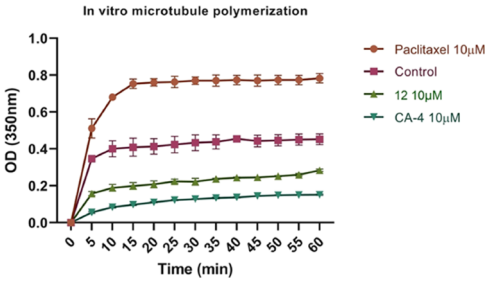

Figure 3. Effect of compound **12** on tubulin polymerization. The experiments were performed three times.

promoting microtubule polymerization, whereas CA-4 produced a noteworthy promotion of microtubule depolymerization. The effect of **12** was similar to CA-4, which indicated that **12** might act as a microtubule depolymerization agent by binding to colchicine sites.

2.2.4. EBI Competition Assay. Consequently, the *N,N′*-ethylenebis(iodoacetamide) (EBI) competition assay was performed to determine whether **12** could bind directly to the colchicine-binding site. As an alkylating reagent, EBI could specifically cross-connect the Cys354 and Cys239 residues of β-tubulin, which were key handles for the binding site of colchicine.[19] EBI could help materialize a β-tubulin adduct that would be prevented by antimitotic agents occupying colchicine-binding sites. As shown in Figure 4, **12** exerted the same inhibitory effect as colchicine to antagonize the generation of the β-tubulin adduct band. This result suggested that **12** could inhibit microtubule polymerization by combining with the colchicine site.

2.2.5. Docking Analysis of 12 with Microtubule. To further describe the potential binding way of **12** to the microtubule, the subunit of the tubulin complex with CA-4 (PDB: 5LYJ) was selected as a template to simulate molecular docking analysis.[20] The result revealed that the indole ring penetrated into the hydrophobic cavity surrounded with residues ASN-258, MET-259, LYS-352, and THR-314 (Figure 5A). The 1-N on the quinazoline scaffold of **12** and the crucial residue Cys 241 constituted a hydrogen bond. **12** and CA-4 shared a remarkably similar combination with the colchicine-binding cavity (Figure 5B). This result indicated that the quinoline scaffold was a substitute for the 3,4,5-trimethoylphenyl fragment and the indole ring substitutes the other benzene ring upon binding to the colchicine site.

2.2.6. 12 Induced G2/M Phase Arrest by Regulating the Related Proteins. Since the majority of antimicrotubule drugs are likely to disrupt cell-cycle distribution,[21] propidium iodide (PI) staining was adopted to detect the performance of **12** on

https://doi.org/10.1021/acs.jmedchem.1c01099
J. Med. Chem. XXXX, XXX, XXX−XXX

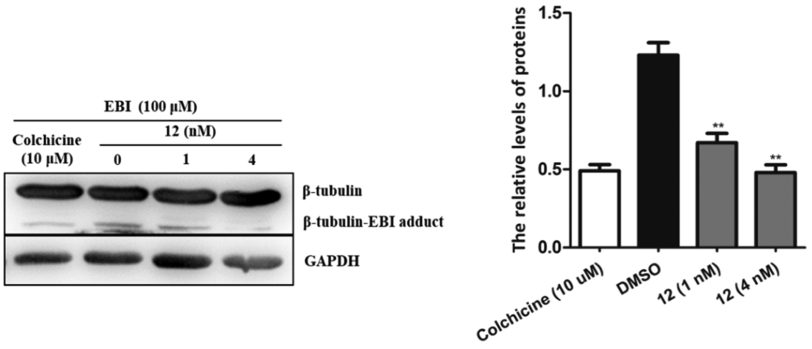

Figure 4. Competition evaluation of **12** and colchicine with EBI on MCF-7 cells. $^{**}p < 0.01$ vs negative control (mean ± SD, $n = 3$).

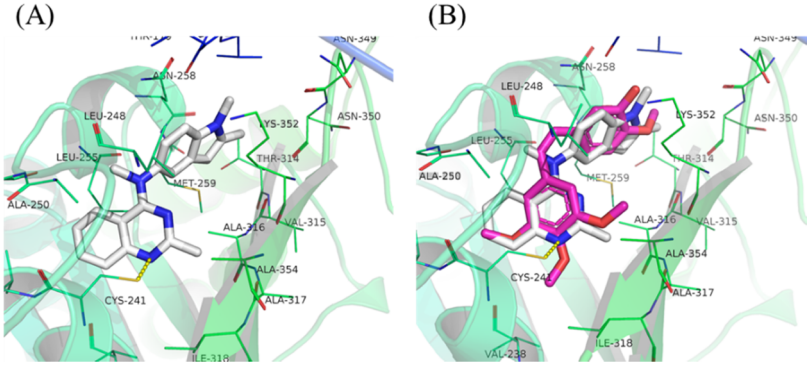

Figure 5. Molecular docking models for **12** binding with microtubule (PDB: 5LYJ). (A) **12** (white). (B) **12** (white) and CA-4 (pink).

the cell-cycle progression of MCF-7. As exhibited in Figure 6A,B, incubation of **12** resulted in G2/M phase arrest. In comparison with the control, the incubation of MCF-7 cells as the concentration of compound **12** increases resulted in the cell percentage increasing from 28.79 to 46.87% in the G2/M phase.

Cyclin B1, Cdc2, and Cdc25c were three important proteins in the cell cycle associated with the G2/M phase. The activation of Cdc2 kinase regulated mitosis in eukaryotic cells, which includes Cdc25c phosphorylation and Cyclin B1 combination.[22] To explore the action of cell-cycle arrest in MCF-7 cells, the effect on cell-cycle-related proteins was evaluated. As shown in Figure 6, **12** decreased the levels of Cdc2 and Cdc25c proteins and increased the levels of Cyclin B1 in a concentration-dependent manner, indicating that the G2/M arrest induced by **12** might be related to the change in expressions of Cyclin B1, Cdc2, and Cdc25c.

*2.2.7. **12** Regulated Apoptosis-Associated Proteins to Induce Apoptosis.* The arrest on cell cycle of tubulin polymerization inhibitors such as CA-4 could lead to cell apoptosis.[23] To determine whether **12** induced apoptosis, dual staining with Annexin V-FITC and propidium iodide (PI) was carried out in MCF-7 cells. As noted in Figure 7, after being exposed to 0.5, 1, and 2 nM **12** for 24 h, the proportions of total apoptotic (Q2 + Q3) MCF-7 cells were 4.45, 35.23, and 57.20%, respectively.

The regulation effects of **12** on apoptosis-related proteins were then analyzed. As shown in Figure 7, **12** decreased the level of Bcl-2 and improved the levels of Bax and Bad, and the levels of cleaved-Caspase-9, cleaved-Caspase-3, and cleaved-PARP were upregulated with the increase in concentration of **12**. The result indicated that compound **12** induced cell apoptosis by affecting the levels of apoptosis-related proteins.

*2.2.8. Effect of **12** on Mitochondrial Membrane Potential (Δψm).* More and more evidence showed that mitochondria played a critical role in the regulation of cell functions, and mitochondrial dysfunction was implicated in apoptosis.[24] To investigate whether **12** could induce mitochondrial dysfunction, JC-1 staining of mitochondria was used to detect the mitochondrial membrane potential in MCF-7. As presented in Figure 8, after MCF-7 cells were administrated with varying concentrations of **12** (0.5, 1, and 2 nM) for 24 h, the green fluorescence intensity (JC-1 monomers, depolarized mitochondria) raised up to 24.7% from 6.49% correspondingly, indicating that **12** might disrupt mitochondrial function to induce breast-cancer-cell apoptosis.

*2.2.9. Action of **12** on Reactive Oxygen Species Accumulation.* The increase of intracellular reactive oxygen species (ROS) in mitochondria could promote the depolarization of the mitochondrial membrane, thus activating the apoptosis of cancer cells.[25] Therefore, we tested whether **12** might stimulate the generation of ROS in MCF-7 cells. As exhibited in Figure 9, the production of intracellular ROS was induced in a concentration-dependent manner, and pretreatment of 2.5 mM *N*-acetylcysteine (ROS scavenging agent) inhibited the increase of ROS.

*2.2.10. **12** Induced Cytostasis and Apoptosis and Inhibited Cell Migration by the Regulation of AhR.* Designed as a dual-target inhibitor, compound **12** was expected to inhibit the AhR/CYP1A1 signaling pathway, thus inducing cell cytostasis. Therefore, Western blot analysis was utilized to measure the levels of AhR and CYP1A1. MCF-7 cells were incubated with varying concentrations (1, 2, 4 nM) of **12** for 24 h, and the AhR antagonist BAY 2416964 was used as a positive control (PC). Then, the levels of AhR and CYP1A1 were detected. The result (Figure 10) showed that as the

https://doi.org/10.1021/acs.jmedchem.1c01099
J. Med. Chem. XXXX, XXX, XXX−XXX

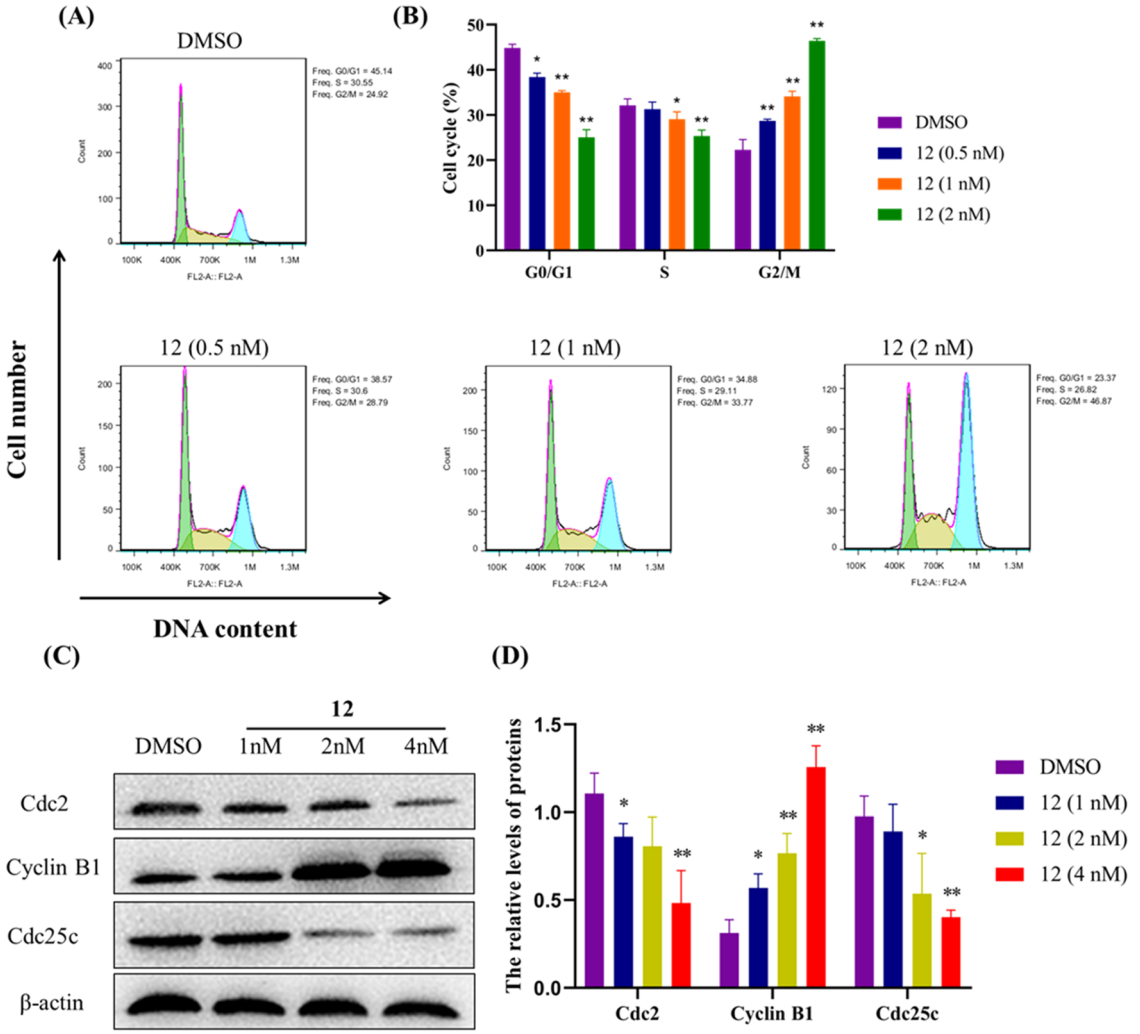

Figure 6. **12** induced G2/M phase arrest in MCF-7 cells. (A) Cells were acquired and then conducted with PI staining and flow cytometry detection. (B) Histograms showing the distribution of the cell cycle (mean ± SD, n = 3). (C) Regulation effects of **12** on the G2/M-related proteins. (D) Histograms showing the relative levels of Cdc2, Cyclin B1, and Cdc25c, to β-actin. *p < 0.05, **p < 0.01 vs the negative control (mean ± SD, n = 3).

concentration increased, the levels of AhR and CYP1A1 continued to decrease, which indicated that **12** could inhibit the AhR/CYP1A1 signaling pathway in a dose-dependent manner.

To investigate whether the regulation of **12** on the AhR/CYP1A1 signaling pathway could inhibit the proliferation of MCF-7 cells, the expression of AhR and proliferation of MCF-7 cells after adding the exogenous AhR agonist 7,12-dimethylbenz[a]anthracene (DMBA) and DMBA+**12** were investigated. The relative expression of AhR in the DMBA+**12** group was notably lower than in the DMBA group (Figure 11A,B), indicating that **12** successfully interfered with the enhanced AhR expression by DMBA. The inhibitory effects of DMBA+**12** on MCF-7 cell proliferation compared with the **12** group further indicated that **12** could inhibit cell proliferation induced by AhR (Figure 11C).

To evaluate whether **12** promoted the apoptosis of MCF-7 cells by synergistically antagonizing microtubule polymerization and AhR expression, the cells were harvested and analyzed by a flow cytometric assay after Annexin V-FITC and PI double staining. As exhibited in Figure 12, the total apoptotic cells in the control, DMBA, DMBA+**12**, and **12** groups were 2.5, 1.5, 27.0, and 51.6%, respectively. The differences between DMBA+**12** and **12** groups indicated that the inhibition of AhR expression was involved in the induction capability of **12** in the apoptosis of MCF-7 cells. Compound **12** could promote apoptosis by synergistically antagonizing microtubule polymerization and AhR expression.

*2.2.11. Effect of **12** on Cell Migration of MCF-7 Cells and AhR Gene Silenced MCF-7 Cells.* Compounds designed to inhibit AhR in this experiment were primarily intended to reduce metastatic transmission of breast cancer cells. Cell migration is an important part of metastatic transmission of tumor cells and the main cause of cancer recurrence.[26] Consequently, we wanted to investigate experimentally whether **12** could inhibit AhR-regulated MCF-7 cell migration while inhibiting tumor growth. As demonstrated in Figure 13, the migration rates of control, DMBA, DMBA+**12**, and **12** groups were 11.51, 12.18, 6.34, and 3.78%, respectively. Compared with the DMBA group (12.18%), the migration rate of the DMBA+**12** group (6.34%) was decreased, which suggested that AhR performed a regulating role in the migration of MCF-7 cells and **12** could partially inhibit the migration of MCF-7 cells through inhibition of AhR.

https://doi.org/10.1021/acs.jmedchem.1c01099
J. Med. Chem. XXXX, XXX, XXX−XXX

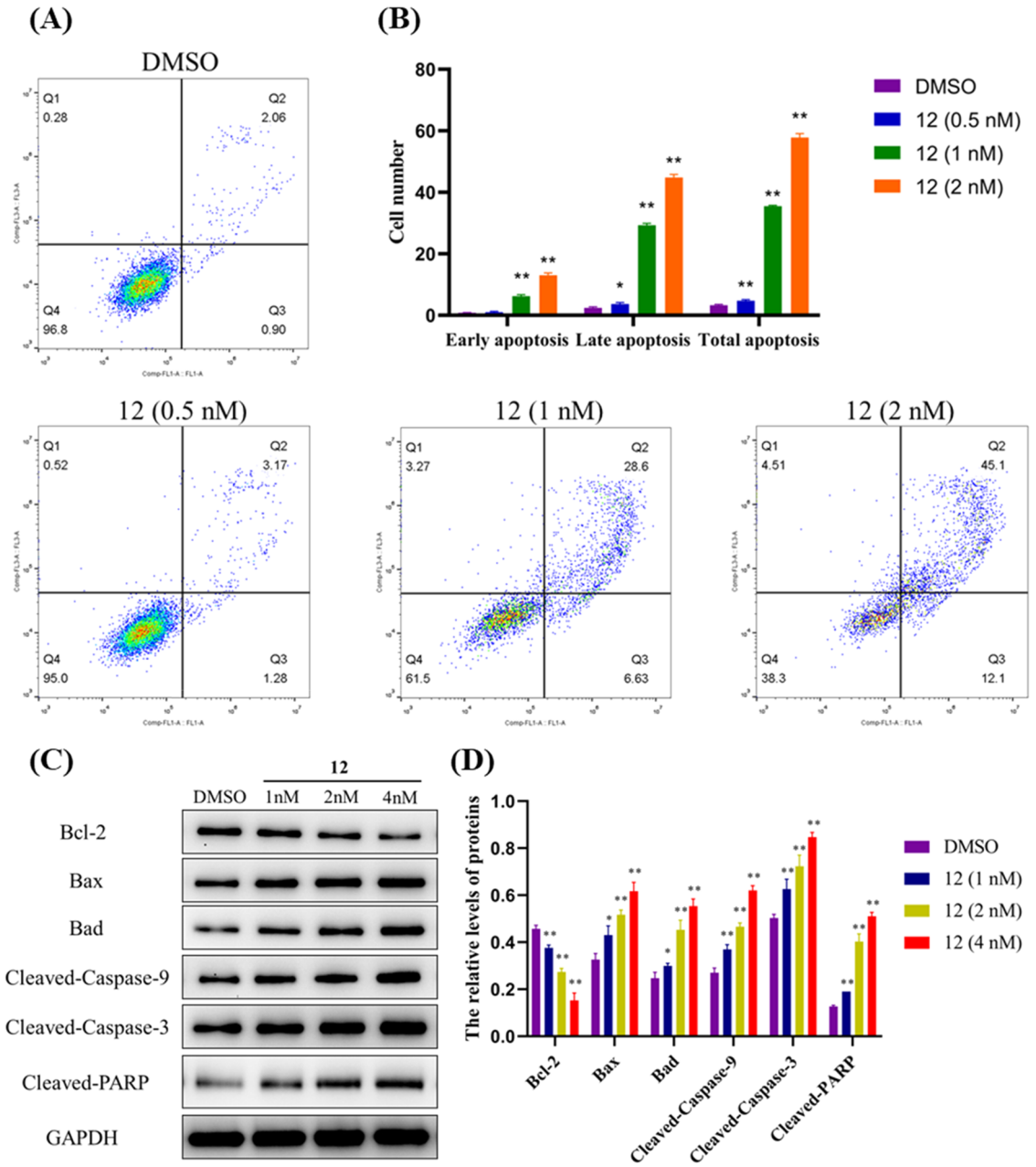

Figure 7. **12** induced apoptosis of MCF-7 cells. (A) Cells were acquired and stained with Annexin V and PI following flow cytometric analysis. (B) Percentage of apoptotic cells was calculated (mean ± SD, $n = 3$). (C) Regulation effects of **12** on apoptosis-related proteins. (D) Relative levels of Bax, Bcl-2, Bad, cleaved-Caspase-9, cleaved-Caspase-3, and cleaved-PARP to GADPH. *$p < 0.05$, **$p < 0.01$ vs the negative control (mean ± SD, $n = 3$).

*2.2.12. Effect of **12** on the Growth of MCF-7 Xenografts in Nude Mice.* To further detect the *in vivo* anticancer potent of **12**, human breast cancer xenograft was established by subcutaneous inoculation of MCF-7 cells into the right side of mice. The animal models were randomly divided into five groups (negative control, paclitaxel, CA-4, low dose of **12**, high dose of **12**) and administered intravenously every 2 days at the indicated doses, with eight mice per group (Figure 14A). Tumor volume and weight of the mice were measured every 2 days. As shown in Figure 14B,D, **12** (1 mg/kg) reduced the tumor weight by 81.1%, which was comparable to PTX (84.2%). Although CA-4 showed excellent inhibitory activity against MCF-7 cells, its anticancer effect (inhibition rate: 37.5% at 20 mg/kg) was less impressive than **12**. Moreover, there was no obvious impact on body weight for **12** at two different doses (Figure 14C). H&E staining of the spleen, lung, liver, heart, and kidney demonstrated no noticeable major organ damage (Figure 15).

Additionally, we observed the effect of **12** on tumor microvessel density (MVD) *in vivo* stained with CD31 by immunohistochemistry. As shown in Figure 16A,B, the MVD was significantly reduced in the **12**-treated group (1 mg/kg). Furthermore, we explored the performance of **12** on apoptosis of tumor cells by Tunel staining. As shown in Figure 16C,D, the cells stained green increased obviously in the tumor treated with **12** (1 mg/kg), which indicated that **12** induced the apoptosis of cells in solid tumors.

https://doi.org/10.1021/acs.jmedchem.1c01099
J. Med. Chem. XXXX, XXX, XXX−XXX

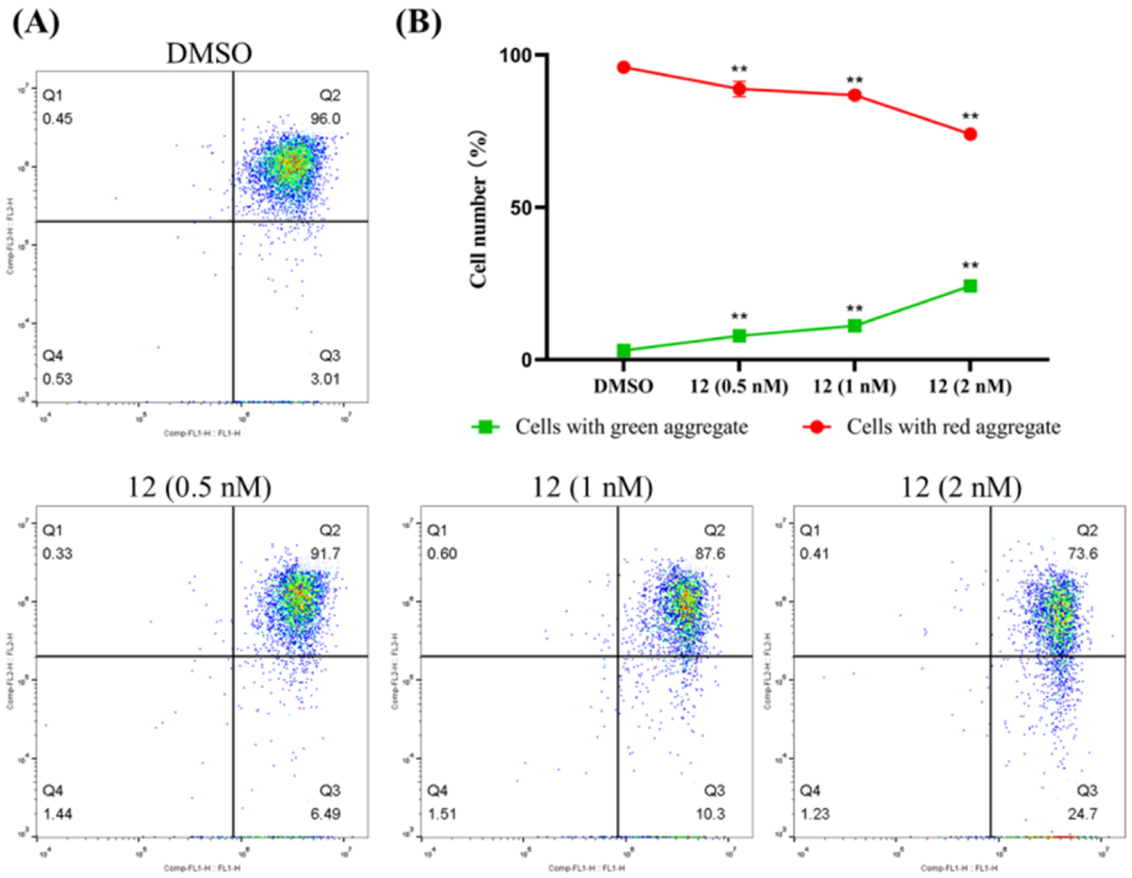

Figure 8. 12 affected the mitochondrial membrane potential of MCF-7 cells. (A) Cells were treated with **12** (0.5, 1, and 2 nM) and DMSO for 24 h prior to staining with JC-1 and then detected by flow cytometry assay. (B) Percentage of cells with *J*-aggregates and *J*-monomers. $^{*}p < 0.05$, $^{**}p < 0.01$ vs the negative control (mean ± SD, $n = 3$).

3. CONCLUSIONS

In conclusion, 12 novel dual-receptor inhibitors targeting both the tubulin colchicine site and AhR were synthesized and evaluated for their antitumor effects. Compared with CA-4 (4.5 nM), compound **12** showed better antitumor ability with an IC_{50} value of 0.9 nM. Furthermore, the inhibitory potent of **12** on microtubule polymerization was investigated by microtubule polymerization, EBI competitive inhibition, intracellular microtubule immunofluorescence, and molecular docking analysis. These assays indicated that **12** significantly inhibited tubulin polymerization by binding to the colchicine site. Further research showed that **12** induced cell-cycle arrest in the G2/M phase and cell apoptosis by regulating the levels of G2/M-related and apoptosis-related proteins. In addition, **12** could depolarize the mitochondrial membrane potential of MCF-7 cells and induce ROS production. Besides, **12** could inhibit the proliferation of MCF-7 cells by synergistically antagonizing microtubule polymerization and AhR expression. The wound healing assay indicated that **12** could inhibit the migration of MCF-7 cells by inhibiting AhR. Moreover, *in vivo* antitumor activities of **12** were verified in MCF-7 breast cancer xenograft mouse models. Most notably, **12** inhibited tumor proliferation with a very small dose (1 mg/kg), while CA-4 had a weak inhibitory effect with a high dose (20 mg/kg). Collectively, these findings indicated that **12** was a novel dual-receptor inhibitor with clinical potential for cancer treatment and warrant further study.

4. EXPERIMENTAL SECTION

4.1. Chemistry. *4.1.1. General Methods.* Target compounds were purified by silica gel column chromatography (200−300 mesh, Qingdao Ocean Chemical Co., Ltd, China). The structures of products were elucidated by characterization with ^{1}H NMR and ^{13}C NMR spectra (AV-300 spectrometer, Bruker Co., Ltd, Germany) in the indicated solvents ($CDCl_3$ or DMSO-d_6). HRMS spectra were detected on a Finnigan MAT 95 spectrometer (Finnigan, Germany). The purity of all inhibitors **1**−**12** was characterized by HPLC analysis (SHIMADZU Prominence-i LC-2030C HPLC system equipped with a PDA detector) to be ≥95%.

4.1.2. General Procedure for the Synthesis of Compounds 1−12. ArCl and aniline derivatives were added successively in isopropanol. One drop of HCl_{conc} was added, and the composites were stirred at 80 °C for 4 h. The residue was washed and dried to obtain the intermediate. The intermediate was mixed into a DMF (5 mL) solution of NaH (3 equiv) at 0 °C. Then, CH_3I (3 equiv) was added at 0 °C and the composites were stirred for 12 h. Further treatment of the crude products by silica gel column chromatography provided target compounds **1**−**12**.

4.1.3. N,2-Dimethyl-N-(3,4,5-trimethoxyphenyl)quinolone-4-amine (1). 3,4,5-Trimethoxyaniline (103 mg, 0.565 mmol) was mixed with 4-chloroquinoline (100 mg, 0.565 mmol) in 10 mL of isopropanol. One drop of HCl_{conc} was added, and the solution was stirred at 80 °C for 4 h. The residue was washed and dried to obtain the intermediate (117 mg). The intermediate was added to a mixture of NaH (26 mg) in DMF (5 mL) at 0 °C. The CH_3I (67 μL) was added dropwise at 0 °C, and the solution was stirred for 12 h. Further treatment of the crude mixture by silica gel column chromatography provided compound **1** (yellow powder, 91 mg, 48% yield). Mp 126.4−128.6 °C; ^{1}H NMR (300 MHz, $CDCl_3$) δ_H: 2.75 (3H, s), 3.47

https://doi.org/10.1021/acs.jmedchem.1c01099
J. Med. Chem. XXXX, XXX, XXX−XXX

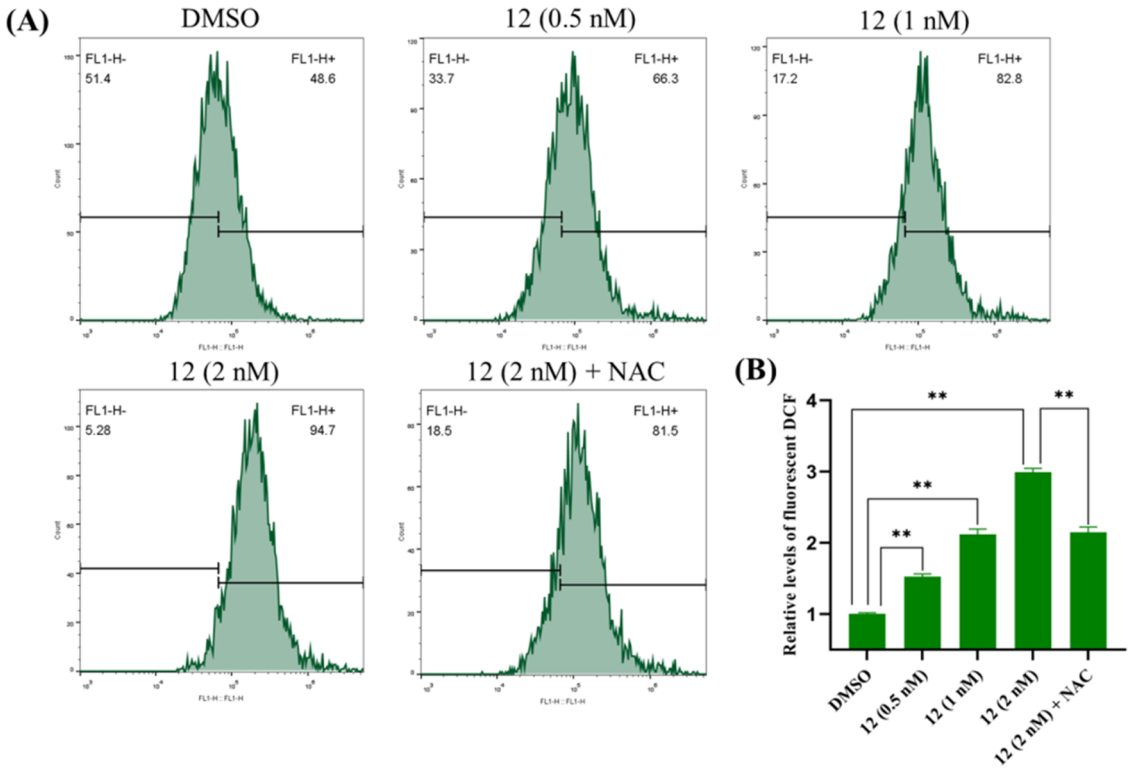

Figure 9. 12 induced ROS accumulation in MCF-7 cells. (A) Generation of ROS was quantified using DCFH-DA followed by FACScan flow cytometry. (B) Relative levels of fluorescent DCF. *p < 0.05, **p < 0.01 vs the negative control (mean ± SD, n = 3).

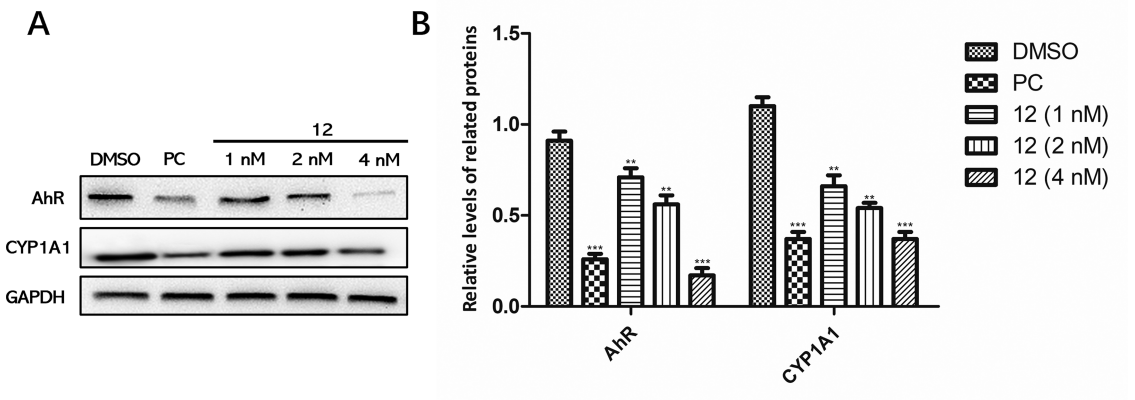

Figure 10. Compound **12** reduced AhR and CYP1A1 expressions in MCF-7 cells. (A, B) Expression and relative levels of AhR/GAPDH and CYP1A1/GAPDH. **p < 0.01, ***p < 0.001 vs the negative control (mean ± SD, n = 3).

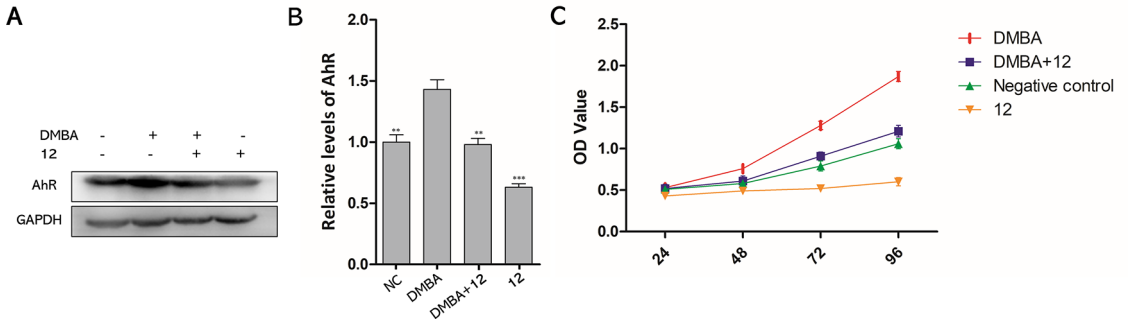

Figure 11. Expression of AhR by adding DMBA (400 nM), DMBA (400 nM)+**12** (2 nM) and **12** (2 nM) in MCF-7 cells. (A, B) Expression and relative levels of AhR. (C) Cell growth curve of MCF-7 cells. **p < 0.01, ***p < 0.001 vs DMBA (mean ± SD, n = 3).

https://doi.org/10.1021/acs.jmedchem.1c01099
J. Med. Chem. XXXX, XXX, XXX−XXX

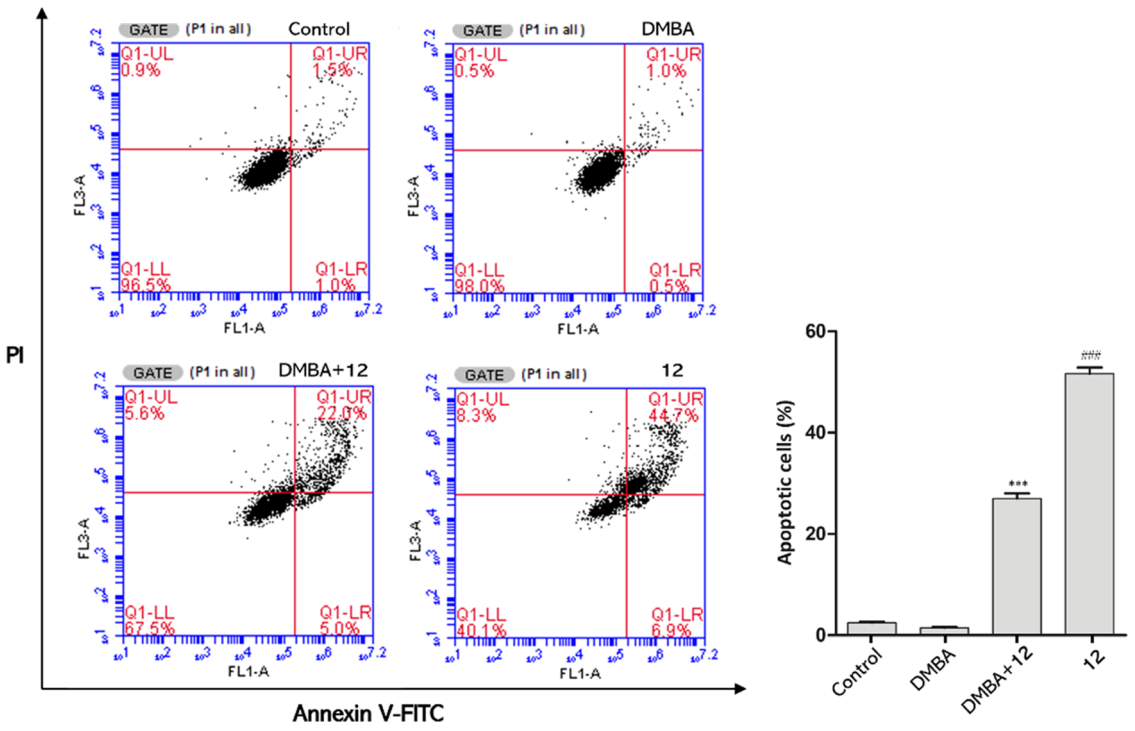

Figure 12. Effects of DMBA (400 nM), DMBA (400 nM)+**12** (2 nM), and **12** (2 nM) on apoptosis of MCF-7 cells. ***$p < 0.001$ vs the DMBA group; $^{###}p < 0.001$ vs the DMBA+**12** group (mean ± SD, $n = 3$).

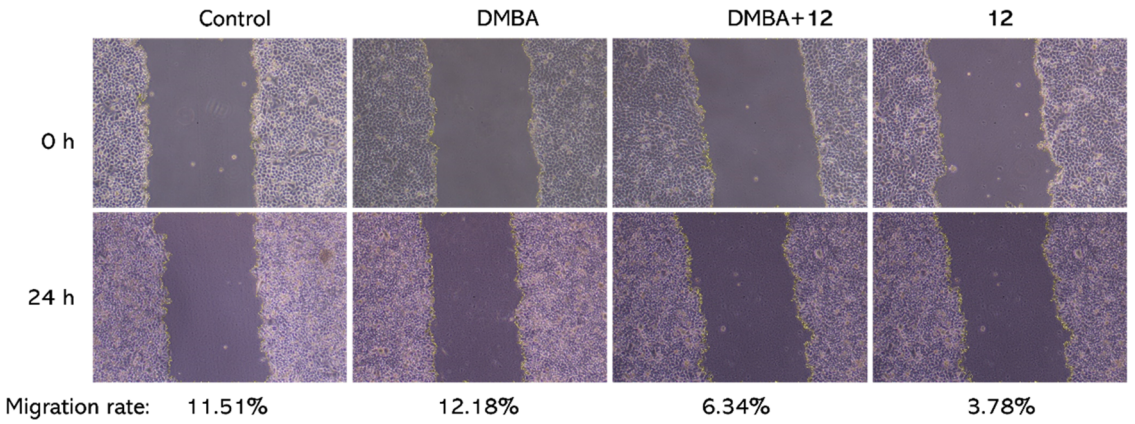

Figure 13. Effect of DMBA (400 nM), DMBA (400 nM)+**12** (2 nM), and **12** (2 nM) on the cell migration of MCF-7 cells. (A) Histograms showing the width of the scratches (0 and 24 h). (B) Migration rate: calculate the area surrounded by cells before and after migration with ImageJ software, and mobility = (area before migration − area after migration)/area before migration.

(3H, s), 3.70 (6H, s), 3.83 (3H, s), 6.14 (2H, s), 7.01 (1H, s), 7.61 (1H, t, J = 7.5 Hz), 7.69 (1H, d, J = 9.0 Hz), 8.03 (1H, d, J = 9.0 Hz); ^{13}C NMR (75 MHz, $CDCl_3$) δ_C: 161.2, 155.6 (C×2), 151.7, 151.4, 147.8, 130.9 (C×2), 130.8, 126.5, 126.1, 124.5, 116.2, 100.1 (C×2), 62.6, 58.0 (C×2), 43.8, 27.0. HRMS (ESI) calculated for $C_{20}H_{22}N_2O_3$ $[M + H]^+$ 339.1709, found 339.1706. Purity: 99.278% (by HPLC).

*4.1.4. N,2-Dimethyl-N-(3,4-dimethoxyphenyl)quinoline-4-amine (**2**).* 3,4-Dimethoxyaniline (86 mg, 0.565 mmol) was mixed into a mixture of 4-chloroquinoline (100 mg, 0.565 mmol) in 10 mL of isopropanol. One drop of HCl_{conc} was added, and the solution was stirred at 80 °C for 4 h. The residue was washed and dried to obtain the intermediate (120 mg). The intermediate was added to a mixture of NaH (29 mg) in DMF (5 mL) at 0 °C. The CH_3I (76 μL) was added at 0 °C, and the solution was stirred for 12 h. Further treatment of the crude mixture by silica gel column chromatography provided compound **2** (brown powder, 94 mg, 54% yield). Mp 99.8−101.4 °C; ^{1}H NMR (300 MHz, DMSO-d_6) δ_H: 2.61 (3H, s), 3.39 (3H, s), 3.65 (3H, s), 3.69 (3H, s), 6.31 (1H, dd, J = 9.0, 3.0 Hz), 6.75−6.79 (2H, m), 7.06 (1H, s), 7.19 (1H, t, J = 7.5 Hz), 7.48−7.55 (2H, m), 7.81 (1H, d, J = 9.0 Hz); ^{13}C NMR (75 MHz, $CDCl_3$) δ_C: 161.0, 155.8, 151.7, 151.1, 147.1, 146.0, 130.7 (C×2), 130.6, 126.4, 126.1, 123.9, 115.0, 114.2, 108.3, 58.1, 57.8, 44.5, 27.0. HRMS (ESI) calculated for $C_{19}H_{20}N_2O_2$ $[M + H]^+$ 309.1603, found 309.1601. Purity: 98.303% (by HPLC).

*4.1.5. N,2-Dimethyl-N-(4-methylphenyl)quinoline-4-amine (**3**).* 4-Methylaniline (60 mg, 0.565 mmol) was mixed into a mixture of 4-chloroquinoline (100 mg, 0.565 mmol) in 10 mL of isopropanol. One drop of HCl_{conc} was added, and the solution was stirred at 80 °C for 4 h. The residue was washed and dried to obtain the intermediate (105 mg). The intermediate was added to a mixture of NaH (31 mg) in DMF (5 mL) at 0 °C. The CH_3I (79 μL) was added at 0 °C, and the solution was stirred for 12 h. Further treatment of the crude mixture by silica gel column chromatography provided compound **3** (yellow powder, 89 mg, 60% yield). Mp 110.3−112.1 °C; ^{1}H NMR (300 MHz, DMSO-d_6) δ_H: 2.21 (3H, s), 2.61 (3H, s), 3.38 (3H, s), 6.77 (2H, d, J = 9.0 Hz), 7.03 (2H, d, J = 9.0 Hz), 7.12 (1H, s), 7.21

https://doi.org/10.1021/acs.jmedchem.1c01099
J. Med. Chem. XXXX, XXX, XXX−XXX

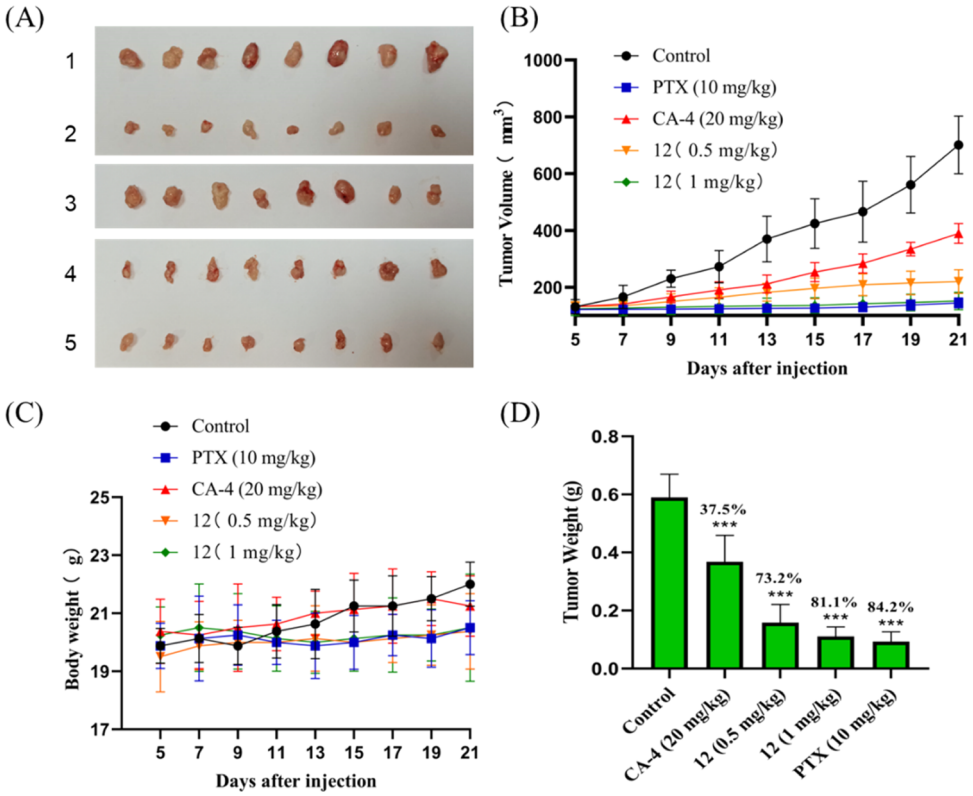

Figure 14. 12 inhibited breast cancer xenograft growth *in vivo*. Negative control (1), paclitaxel (PTX) (10 mg/kg, 2), CA-4 (20 mg/kg, 3), **12** (0.5 mg/kg, 4), and **12** (1 mg/kg, 5). (A) Images of tumors at 3 weeks after initiation of drug administration. (B) Changes of compound administration on tumor size in mice. (C) Changes of compound administration on mice body weight. (D) Weight of the excised tumors of each group. ***p < 0.001 vs control.

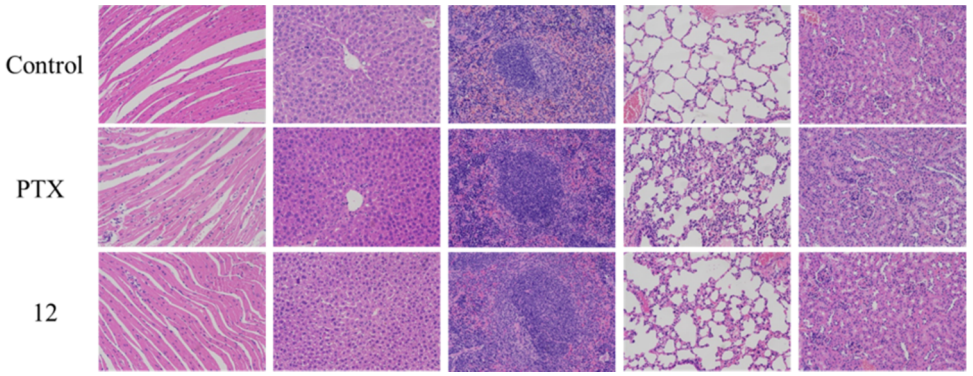

Figure 15. H&E staining of the heart, liver, spleen, lung, and kidney of mice.

(1H, t, J = 9.0 Hz), 7.50 (1H, d, J = 9.0 Hz), 7.56 (1H, d, J = 9.0 Hz), 7.84 (1H, d, J = 9.0 Hz); ^{13}C NMR (75 MHz, $CDCl_3$) δ_C: 161.3, 155.9, 151.5, 149.5, 132.9, 131.6 (C×2), 130.9, 130.7, 126.3 (C×2), 124.6, 121.5 (C×2), 116.0, 43.7, 27.1, 22.2. HRMS (ESI) calculated for $C_{18}H_{18}N_2$ $[M + H]^+$ 263.1548, found 263.1543. Purity: 99.347% (by HPLC).

*4.1.6. N,2-Dimethyl-N-(3,4-methylenedioxyphenyl)quinoline-4-amine (**4**).* 3,4-Methylenedioxyaniline (77 mg, 0.565 mmol) was mixed into a mixture of 4-chloroquinoline (100 mg, 0.565 mmol) in 10 mL of isopropanol. One drop of HCl_{conc} was added, and the solution was stirred at 80 °C for 4 h. The residue was washed and dried to obtain the intermediate (110 mg). The intermediate was added to a mixture of NaH (28 mg) in DMF (5 mL) at 0 °C. The CH_3I (74 μL) was added at 0 °C, and the solution was stirred for 12 h. Further treatment of the crude mixture by silica gel column chromatography provided compound **4** (brown powder, 81 mg, 49% yield). Mp 71.8−73.2 °C; ^{1}H NMR (300 MHz, DMSO-d_6) δ_H: 2.61 (3H, s), 3.35 (3H, s), 5.98 (2H, s), 6.29 (1H, dd, J = 9.0, 3.0 Hz), 6.68 (1H, d, J = 3.0 Hz), 6.75 (1H, d, J = 9.0 Hz), 7.08 (1H, s), 7.23 (1H, t, J = 7.5 Hz), 7.52−7.56 (2H, m), 7.83 (1H, d, J = 9.0 Hz); ^{13}C NMR (75 MHz, $CDCl_3$) δ_C: 161.2, 155.8, 151.5, 150.2, 147.2, 144.9, 130.9, 130.6, 126.3, 126.2, 124.2, 115.4, 114.8, 110.2, 104.9, 103.0, 44.5, 27.1. HRMS (ESI) calculated for $C_{18}H_{16}N_2O_2$ $[M + H]^+$ 293.1290, found 293.1287. Purity: 98.459% (by HPLC).

*4.1.7. N,2-Dimethyl-N-(4-trifluoromethylphenyl)quinoline-4-amine (**5**).* 4-Trifluoromethylaniline (91 mg, 0.565 mmol) was mixed into a mixture of 4-chloroquinoline (100 mg, 0.565 mmol) in 10 mL of isopropanol. One drop of HCl_{conc} was added, and the solution was stirred at 80 °C for 4 h. The residue was washed and dried to obtain the intermediate (137 mg). The intermediate was added to a mixture of NaH (33 mg) in DMF (5 mL) at 0 °C. The CH_3I (84 μL) was added at 0 °C, and the solution was stirred for 12 h. Further treatment of the crude mixture by silica gel column chromatography provided compound **5** (white powder, 121 mg, 68%

https://doi.org/10.1021/acs.jmedchem.1c01099
J. Med. Chem. XXXX, XXX, XXX−XXX

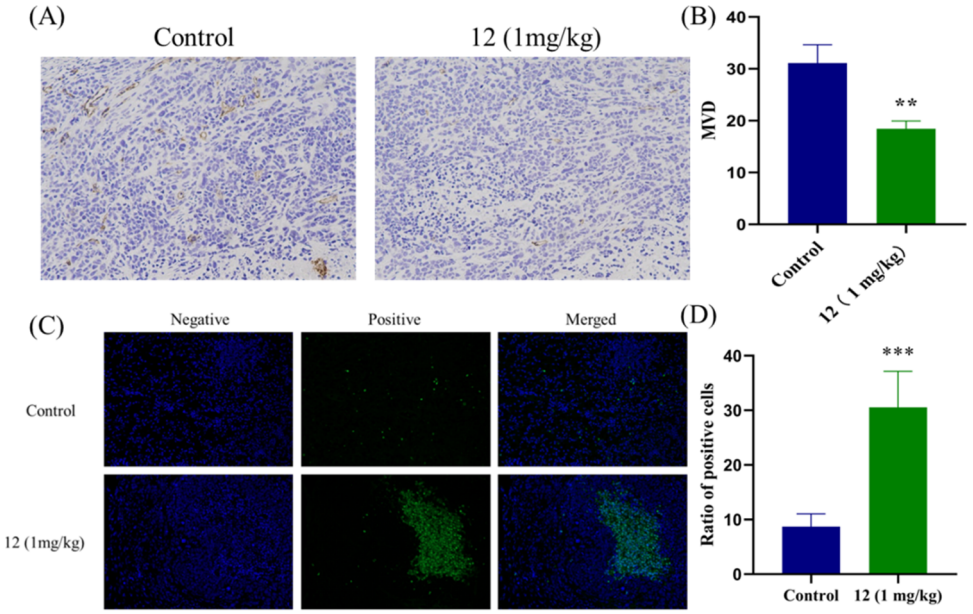

Figure 16. Tumor section staining. (A) Typical anti-CD31 immunohistochemistry images from four MCF-7 xenografts. (B) MVD measured by immunohistochemical staining against CD31 in MCF-7 xenografts administrated with a negative control and **12** (1 mg/kg). $^{**}p < 0.01$ vs the negative control. (C) Representative images of TUNEL fluorescent staining from four tumor xenografts. DNA was stained blue, and the apoptotic cells were stained green. (D) Ratio of positive cells by TUNEL fluorescent staining. $^{***}p < 0.001$ vs the negative control.

yield). Mp 129.6−132.4 °C; ^{1}H NMR (300 MHz, DMSO-d_6) δ_H: 2.66 (3H, s), 3.45 (3H, s), 6.77 (2H, d, J = 9.0 Hz), 7.39 (1H, s), 7.41−7.49 (3H, m), 7.62 (1H, d, J = 9.0 Hz), 7.70 (1H, t, J = 7.5 Hz), 7.99 (1H, d, J = 9.0 Hz); ^{13}C NMR (75 MHz, $CDCl_3$) δ_C: 160.2, 152.7, 151.4, 149.9, 129.9 (C×2), 129.4 (C×2), 126.4, 126.4, 125.9, 123.6, 123.4, 118.8, 114.9 (C×2), 40.5, 25.3. HRMS (ESI) calculated for $C_{18}H_{15}F_3O_2$ $[M + H]^+$ 317.1266, found 317.1266. Purity: 99.485% (by HPLC).

*4.1.8. N,2-Dimethyl-N-(4-biphenylyl)quinoline-4-amine (**6**).* 4-Biphenylamine (96 mg, 0.565 mmol) was mixed into a mixture of 4-chloroquinoline (100 mg, 0.565 mmol) in 10 mL of isopropanol. One drop of HCl_{conc} was added, and the solution was stirred at 80 °C for 4 h. The residue was washed and dried to obtain the intermediate (140 mg). The intermediate was added to a mixture of NaH (33 mg) in DMF (5 mL) at 0 °C. The CH_3I (84 μL) was added at 0 °C, and the mixture was stirred for 12 h. Further treatment of the crude mixture by silica gel column chromatography provided compound **6** (yellow powder, 103 mg, 56% yield). Mp 135.8−137.4 °C; ^{1}H NMR (300 MHz, DMSO-d_6) δ_H: 2.65 (3H, s), 3.47 (3H, s), 6.88 (2H, d, J = 9.0 Hz), 7.26−7.43 (5H, m), 7.53 (2H, d, J = 6.0 Hz), 7.58−7.65 (4H, m), 7.93 (1H, d, J = 9.0 Hz); ^{13}C NMR (75 MHz, $CDCl_3$) δ_C: 159.7, 153.8, 149.6, 148.8, 140.6, 133.7, 129.4, 128.7 (C×2), 127.8 (C×2), 126.7, 126.5 (C×2), 125.1, 124.3, 123.1, 118.5 (C×2), 115.9, 41.5, 25.3. HRMS (ESI) calculated for $C_{23}H_{20}N_2$ $[M + H]^+$ 325.1705, found 325.1704. Purity: 99.161% (by HPLC).

*4.1.9. N,2-Dimethyl-N-(4-N,N-dimethylaminophenyl)quinoline-4-amine (**7**).* *N,N*-Dimethyl-1,4-phenylenediamine (77 mg, 0.565 mmol) was mixed into a mixture of 4-chloroquinoline (100 mg, 0.565 mmol) in 10 mL of isopropanol. One drop of HCl_{conc} was added, and the solution was stirred at 80 °C for 4 h. The residue was washed and dried to obtain the intermediate (102 mg). The intermediate was added to a mixture of NaH (26 mg) in DMF (5 mL) at 0 °C. The CH_3I (69 μL) was added at 0 °C, and the mixture was stirred for 12 h. Further treatment of the crude mixture by silica gel column chromatography provided compound **7** (brown powder, 64 mg, 39% yield). Mp 99.6−101.4 °C; ^{1}H NMR (300 MHz, $CDCl_3$) δ_H: 2.72 (3H, s), 2.93 (6H, s), 3.41 (3H, s), 6.68 (2H, d, J = 9.0 Hz), 6.86 (1H, s), 6.93 (2H, d, J = 9.0 Hz), 7.15 (1H, t, J = 7.5 Hz), 7.52 (1H, t, J = 7.5 Hz), 7.61 (1H, d, J = 9.0 Hz), 7.96 (1H, d, J = 9.0 Hz); ^{13}C NMR (75 MHz, $CDCl_3$) δ_C: 159.0, 154.2, 149.1, 147.4, 140.7, 128.7, 128.5, 125.2, 123.9, 123.8 (C×2), 121.6, 113.7 (C×2), 110.4, 43.3, 40.9 (C×2), 25.3. HRMS (ESI) calculated for $C_{19}H_{21}N_3$ $[M + H]^+$ 292.1814, found 292.1812. Purity: 99.077% (by HPLC).

*4.1.10. N,2-Dimethyl-N-(4-N,N-diethylaminophenyl)quinoline-4-amine (**8**).* *N,N*-Diethyl-1,4-phenylenediamine (93 mg, 0.565 mmol) was mixed into a mixture of 4-chloroquinoline (100 mg, 0.565 mmol) in 10 mL of isopropanol. One drop of HCl_{conc} was added, and the solution was stirred at 80 °C for 4 h. The residue was washed and dried to obtain the intermediate (138 mg). The intermediate was added to a mixture of NaH (33 mg) in DMF (5 mL) at 0 °C. The CH_3I (84 μL) was added at 0 °C, and the solution was stirred for 12 h. Further treatment of the crude mixture by silica gel column chromatography provided compound **8** (brown powder, 43 mg, 24% yield). Mp 118.7−120.3 °C; ^{1}H NMR (300 MHz, $CDCl_3$) δ_H: 1.16 (6H, t, J = 6.0 Hz), 2.72 (3H, s), 3.33 (4H, d, J = 6.0 Hz), 3.41 (3H, s), 6.62 (2H, d, J = 9.0 Hz), 6.84 (1H, s), 6.91 (2H, d, J = 9.0 Hz), 7.15 (1H, t, J = 7.5 Hz), 7.52 (1H, t, J = 7.5 Hz), 7.64 (1H, d, J = 9.0 Hz), 7.95 (1H, d, J = 9.0 Hz); ^{13}C NMR (75 MHz, $CDCl_3$) δ_C: 159.0, 154.2, 144.8, 139.9, 130.9, 128.6, 128.5, 125.3, 124.1 (C×2), 123.8, 121.6, 113.2 (C×2), 110.13, 44.5 (C×2), 43.4, 25.4, 12.6 (C×2). HRMS (ESI) calculated for $C_{21}H_{25}N_3$ $[M + H]^+$ 320.2127, found 320.2126. Purity: 98.652% (by HPLC).

*4.1.11. N,2-Dimethyl-N-(1-methyl-7-azaindole-5-yl)quinoline-4-amine (**9**).* 7-Azazindole-5-amine (75 mg, 0.565 mmol) was mixed into a mixture of 4-chloroquinoline (100 mg, 0.565 mmol) in 10 mL of isopropanol. One drop of HCl_{conc} was added, and the solution was stirred at 80 °C for 4 h. The residue was washed and dried to obtain the intermediate (132 mg). The intermediate was added to a mixture of NaH (35 mg) in DMF (5 mL) at 0 °C. The CH_3I (90 μL) was added at 0 °C, and the solution was stirred for 12 h. Further treatment of the crude mixture by silica gel column chromatography provided compound **9** (yellow powder, 29 mg, 17% yield). Mp 83.5−85.8 °C; ^{1}H NMR (300 MHz, DMSO-d_6) δ_H: 2.74 (3H, s), 3.51 (3H, s), 3.89 (3H, s), 6.32 (1H, d, J = 3.0 Hz), 6.95 (1H, s), 7.15 (1H, t, J = 7.5 Hz), 7.18 (1H, d, J = 3.0 Hz), 7.48−7.53 (2H, m), 7.60 (1H, d, J = 9.0 Hz), 7.96 (1H, d, J = 9.0 Hz), 8.20 (1H, d, J = 3.0 Hz); ^{13}C NMR (75 MHz, $CDCl_3$) δ_C: 161.00 156.0, 146.8, 142.9, 141.2, 131.8, 130.8, 130.5, 126.6, 126.1, 123.6, 123.4, 122.3, 113.4, 111.8, 100.9, 45.6, 32.9, 27.2. HRMS (ESI) calculated for $C_{19}H_{18}N_4$ $[M + H]^+$ 303.1610, found 303.1608. Purity: 99.533% (by HPLC). Solubility (H_2O, 2.23 mg/mL).

https://doi.org/10.1021/acs.jmedchem.1c01099
J. Med. Chem. XXXX, XXX, XXX−XXX

*4.1.12. N,2-Dimethyl-N-(1,2-dimethylindol-5-yl)quinoline-4-amine (**10**).* 5-Amino-2-methylindole (83 mg, 0.565 mmol) was mixed into a mixture of 4-chloroquinoline (100 mg, 0.565 mmol) in 10 mL of isopropanol. One drop of HCl_{conc} was added, and the solution was stirred at 80 °C for 4 h. The residue was washed and dried to obtain the intermediate (127 mg). The intermediate was added to a solution of NaH (32 mg) in DMF (5 mL) at 0 °C. The CH_3I (82 μL) was added at 0 °C, and the solution was stirred for 12 h. Further treatment of the crude mixture by silica gel column chromatography provided compound **10** (yellow powder, 28 mg, 16% yield). Mp 120.9−123.3 °C; ^{1}H NMR (300 MHz, DMSO-d_6) δ_H: 2.35 (3H, s), 2.62 (3H, s), 3.40 (3H, s), 3.62 (3H, s), 6.07 (1H, s), 6.84 (1H, dd, J = 9.0, 3.0 Hz), 6.98−7.01 (3H, m), 7.31 (1H, d, J = 9.0 Hz), 7.41−7.46 (2H, m), 7.76 (1H, d, J = 6.0 Hz); ^{13}C NMR (75 MHz, $CDCl_3$) δ_C: 158.9, 154.7, 143.7, 137.9, 134.6, 128.6 (C×2), 128.4, 125.4 (C×2), 123.8, 121.6, 117.4, 114.1, 110.1, 109.5, 99.7, 44.1, 29.5, 25.3, 12.7. HRMS (ESI) calculated for $C_{21}H_{21}N_3$ $[M + H]^+$ 316.1814, found 316.1812. Purity: 99.694% (by HPLC).

*4.1.13. N,2-Dimethyl-N-(1-methyl-7-azaindole-5-yl)quinazoline-4-amine (**11**).* 7-Azazindole-5-amine (75 mg, 0.562 mmol) was mixed into a mixture of 4-chloroquinazoline (100 mg, 0.562 mmol) in 10 mL of isopropanol. One drop of HCl_{conc} was added, and the solution was stirred at 80 °C for 4 h. The residue was washed and dried to obtain the intermediate (145 mg). The intermediate was added to a mixture of NaH (38 mg) in DMF (5 mL) at 0 °C. The CH_3I (99 μL) was added at 0 °C, and the solution was stirred for 12 h. Further treatment of the crude mixture by silica gel column chromatography provided compound **11** (brown powder, 40 mg, 24% yield). Mp 172.5−174.4 °C; ^{1}H NMR (300 MHz, DMSO-d_6) δ_H: 2.61 (3H, s), 3.58 (3H, s), 3.84 (3H, s), 6.46 (1H, d, J = 3.0 Hz), 6.86 (1H, d, J = 6.0 Hz), 6.97 (1H, t, J = 7.5 Hz), 7.56 (1H, t, J = 7.5 Hz), 7.61 (1H, d, J = 3.0 Hz), 7.67 (1H, d, J = 6.0 Hz), 7.92 (1H, d, J = 3.0 Hz), 8.18 (1H, d, J = 3.0 Hz); ^{13}C NMR (75 MHz, $CDCl_3$) δ_C: 163.3, 161.9, 152.2, 146.1, 141.4, 138.6, 131.7, 130.7, 127.7, 126.1, 125.9, 124.1, 120.8, 114.5, 99.7, 43.6, 31.4, 26.4. HRMS (ESI) calculated for $C_{18}H_{17}N_5$ $[M + H]^+$ 304.1562, found 304.1560. Purity: 96.734% (by HPLC).

*4.1.14. N,2-Dimethyl-N-(1,2-dimethylindol-5-yl)quinazoline-4-amine (**12**).* 5-Amino-2-methylindole (74 mg, 0.562 mmol) was mixed into a mixture of 4-chloroquinazoline (100 mg, 0.562 mmol) in 10 mL of isopropanol. One drop of HCl_{conc} was added, and the solution was stirred at 80 °C for 4 h. The residue was washed and dried to obtain the intermediate (154 mg). The intermediate was added to a mixture of NaH (38 mg) in DMF (5 mL) at 0 °C. The CH_3I (100 μL) was added at 0 °C, and the solution was stirred for 12 h. Further treatment of the crude mixture by silica gel column chromatography provided compound **12** (white powder, 51 mg, 29% yield). Mp 218.5−220.2 °C; ^{1}H NMR (300 MHz, DMSO-d_6) δ_H: 2.41 (3H, s), 2.59 (3H, s), 3.55 (3H, s), 3.69 (3H, s), 6.19 (1H, s), 6.84−6.91 (2H, m), 6.96−6.99 (1H, dd, J = 9.0, 3.0 Hz), 7.30 (1H, s), 7.45 (1H, d, J = 9.0 Hz), 7.47−7.53 (1H, m), 7.61 (1H, d, J = 9.0 Hz); ^{13}C NMR (75 MHz, DMSO-d_6) δ_C: 162.8, 161.6, 152.2, 140.5, 139.3, 136.0, 132.0, 128.7, 127.8, 126.4, 124.1, 119.0, 116.9, 114.9, 111.1, 100.1, 43.5, 29.9, 26.6, 12.9. HRMS (ESI) calculated for $C_{20}H_{20}N_4$ $[M + H]^+$ 317.1766, found 317.1764. Purity: 96.734% (by HPLC).

4.2. Biological Evaluation. *4.2.1. Materials.* EBI and the purified tubulin polymerization kit were bought from Cytoskeleton Inc. (Denver). The annexin V-FITC apoptosis detection kit, 3-(4,5-dimethylthiazol-2-yl)-2,5-diphenyl-2-*H*-tetrazolium bromide (MTT), propidium iodide (PI), JC-1, DMEM, and RPMI 1640 medium were bought from Nanjing KeyGen Biotech Co. Ltd. (Nanjing, China). Primary antibodies against Cdc2, Cdc25c, Bax, Bad, Cyclin B1, Bcl-2, cleaved-Caspase-3, cleaved-Caspase-9, cleaved-PARP, AhR, and CYP1A1 were bought from Beyotime (Shanghai, China). Goat antirabbit IgG/Alexa-Fluor 488 antibody was bought from Jackson ImmunoResearch Inc. (West Grove).

4.2.2. Cell Lines and Cell Culture. Human breast cancer cells (MCF-7), human normal hepatocyte cells (L-O2), and hepatocellular carcinoma cells (HepG-2) were cultured in DMEM medium. Human lung cancer cells (A549), human normal mammary cells (MCF-10A), and adriamycin-resistant human breast cancer cells (MCF-7/ADR) were cultured in RPMI 1640 medium.

4.2.3. MTT Assay. The proliferation activity of human tumor cell lines (MCF-7, HepG-2, A549, MCF-7/ADR) and human normal cells (MCF-10A, L-O2) was measured using the MTT assay. Cells (5×10^3 cells per well) were plated in 96-well plates. After being incubated overnight, cells were administrated with target compounds at varying concentrations and incubated for 48 h. Then, the plates were incubated for 4 h after the MTT solution was added. After that, the culture medium was replaced with 100 μL of dimethyl sulfoxide. The absorbance was quantitatively detected by a microplate reader (Biorad, Nazareth, Belgium) at 570 nm. All experiments were carried out three times.

4.2.4. Immunofluorescent Staining. MCF-7 cells were incubated in six-well plates (4×10^5 cells) and then given DMSO, **12** (0.5, 1, 2, 4 nM), and colchicine (200 nM) for 48 h. After being treated with goat serum albumin (50−100 μL) for 20 min, cells were cultured with anti-β-tubulin for 2 h. After fluorescent antibody staining and 4,6-diamino-2-phenylindole (DAPI) labeling of the nucleus, the plates were washed with PBS three times. Cells were subsequently monitored by employing an LSM 570 laser confocal microscope (Carl Zeiss, Germany).

4.2.5. Evaluation of Tubulin Polymerization Inhibition In Vitro. In PEM buffer, 2 mg/mL tubulin (cytoskeleton) was resuspended. Then, the suspension was preincubated on ice with target products or the vehicle DMSO. Before monitoring the tubulin polymerization reaction, PEG was added to make the ultimate concentration 3 mg/mL. The absorbance was recorded every 5 min for 60 min at 37 °C by a spectrophotometric operation at 350 nm.

4.2.6. EBI Competition Evaluation. MCF-7 cells were incubated in six-well cell culture plates (5×10^5 cells) for 24 h. Then, cells were first incubated with DMSO, **12** (1, 4 nM), and colchicine (10 μM) for 2 h, followed by processing with EBI (100 μM). After that, the cells were collected and cell extracts were employed for the Western blot assay.

4.2.7. Molecular Docking Analysis. The X-ray crystal structure of the α,β-tubulin−CA-4 complex (PDB ID: 5LYJ) was obtained from the Protein Data Bank. Discovery Studio modules were employed to prepare the complex by removing the stathmin-like domain, colchicine, water molecules, and subunits C and D. The mimic procedure was carried out using the DOCK system in Discovery Studio 3.0 software, and the generating graphics were acquired from PyMOL software.

4.2.8. Cell-Cycle Assay. MCF-7 cells were incubated in six-well cell culture plates for 24 h (4×10^5 cells). Then, DMSO and **12** (0.5, 1, and 2 nM) were added to the plates. After that, cells were mixed with ethyl alcohol (75%) at −20 °C for 12 h. Next, the plates were washed with buffer A to remove ethanol. Staining was performed according to the cell-cycle analysis kit, and then, analysis was performed with a flow cytometric assay. The assay was carried out 3 times.

4.2.9. Cell Apoptosis Evaluation. MCF-7 cells were incubated in six-well cell culture plates for 24 h (4×10^5 cells). Then, DMSO and **12** (0.5, 1, and 2 nM) were dropped into each well. After the next culturation of 24 h, cells were collected and cleaned twice with PBS (2000 rpm + 5 min). After that, the cells were resuspended in 500 μL of binding buffer; then, 5 μL of annexin and 5 μL of propidium iodide were added one by one. The mixed solution was incubated for 15 min in the shade and detected by a flow cytometric assay. The assay was carried out 3 times.

4.2.10. Mitochondrial Membrane Potential Evaluation. The MCF-7 cell suspension was inoculated into six-well plates for 24 h (4×10^5 cells). Then, cells were cultured in a fresh medium with dimethyl sulfoxide and **12** (0.5, 1, and 2 nM) for another 24 h. After the next culturation of 24 h, cells were collected and cleaned twice with PBS (2000 rpm + 5 min), followed by incubation with JC-1 (5 mg/mL) for 30 min shielded from light. After rinsing 3 times, the cells were suspended in PBS, and the fluorescence of JC-1 was detected by a flow cytometric assay. The assay was carried out 3 times.

https://doi.org/10.1021/acs.jmedchem.1c01099
J. Med. Chem. XXXX, XXX, XXX−XXX

4.2.11. Measurement of Intracellular ROS Generation. The MCF-7 cell suspension was inoculated into six-well plates for 24 h (4×10^5 cells). Then, cells were cultured in a fresh medium with dimethyl sulfoxide and **12** (0.5, 1, and 2 nM) for another 24 h. After that, cells were cultured with DCFH-DA for 30 min shielded from light. Then, cells were suspended in a medium with no fetal bovine serum and detected by a flow cytometric assay. Cells were treated with 2.5 mM *N*-acetyl-L-cysteine and then cultured with 2 nM **12** for another 24 h. The assay was carried out 3 times.

4.2.12. Western Blotting Assay. The MCF-7 cell suspension was inoculated into six-well plates for 24 h (4×10^5 cells). Then, cells were cultured in a fresh medium with dimethyl sulfoxide and **12** (1, 2, and 4 nM) for 24 h. Cells were incubated and lysed with the lysis buffer, and proteins were extracted. After that, proteins were diluted to 3 mg/mL based on the BCA protein assay kit (Beyotime, China). Each sample (10 μL) was detected by SDS-PAGE (4−20% gel). The assay was carried out 3 times.

4.2.13. Cell Migration Inhibition Assay. The MCF-7 cell suspension was seeded into six-well cell plates for 24 h (5×10^5 cells). After cells were attached to the plate, a sterile pipette tip was used to scrape the bottom of each hole to destroy the monolayer cells. Then, the graphics were taken under an inverted fluorescence microscope. After that, DMSO, DMBA, DMBA+**12** and **12** (2 nM) were added to each well. Photos were taken at fixed positions at 24 h, and results were analyzed by ImageJ software.

4.2.14. Evaluation of Antitumor Activity In Vivo. The right side of Bal b/c nude mice was inoculated subcutaneously with 6×10^6 MCF-7 cells based on the protocols of the tumor transplantation analysis. After culturation for 7 days, the weights of mice were recorded, and then, the mice were randomly separated into five groups (eight animals per group). Group 1 was administrated with 10% DMSO/5% Tween 80/85% saline through intravenous injection (iv). Group 2 was administrated with PTX (10 mg/kg per 2 days) through intravenous administration. Group 3 was administrated with CA-4 (20 mg/kg per 2 days) through iv. Group 4 was administrated with **12** (0.5 mg/kg every 2 days) through iv. Group 5 was administrated with **12** (1 mg/kg every 2 days) through iv. Tumor sizes and body weights were detected every 2 days. All of the mice were killed after administration for 21 consecutive days and then weighed. Tumor volumes were calculated by employing the following formula: $V = L \times W^2/2$, with V (mm^3) being the volume, W (mm) being the width, and L (mm) being the length of the tumor. The tumors and organs were fixed, paraffin-embedded, and sectioned. The tumor tissue sections were stained with the TUNEL kit to observe the proportion of apoptotic cells; pathologic staining of major tissues and organs was performed using hematoxylin and eosin (HE) staining; CD31 staining was used to calculate the mean microvascular density. All procedures were carried out following institutional approval for the Care and Use of Laboratory Animals.

■ ASSOCIATED CONTENT

Supporting Information

The Supporting Information is available free of charge at https://pubs.acs.org/doi/10.1021/acs.jmedchem.1c01099.

Structural characterization of **1**−**12** (^{1}H NMR, ^{13}C NMR, ESI/HRMS spectra); and HPLC analyses of **1**−**12** (PDF)

Molecular string files for **1**−**12** (CSV)

■ AUTHOR INFORMATION

Corresponding Authors

Li Chen − *State Key Laboratory of Natural Medicines, Department of Natural Medicinal Chemistry, School of Traditional Chinese Pharmacy, China Pharmaceutical University, Nanjing 210009, China*; orcid.org/0000-0002-4655-9024; Phone: +86-25-83271447; Email: chenli627@cpu.edu.cn

Jianbo Sun − *State Key Laboratory of Natural Medicines, Department of Natural Medicinal Chemistry, School of Traditional Chinese Pharmacy, China Pharmaceutical University, Nanjing 210009, China*; Phone: +86-25-83271415; Email: sunjianbo@cpu.edu.cn

Authors

Kun Wang − *State Key Laboratory of Natural Medicines, Department of Natural Medicinal Chemistry, School of Traditional Chinese Pharmacy, China Pharmaceutical University, Nanjing 210009, China*

Hui Zhong − *Department of Pharmacology of Traditional Chinese Medicine, School of Traditional Chinese Pharmacy, China Pharmaceutical University, Nanjing 210009, China*

Na Li − *State Key Laboratory of Natural Medicines, Department of Natural Medicinal Chemistry, School of Traditional Chinese Pharmacy, China Pharmaceutical University, Nanjing 210009, China*

Nairong Yu − *State Key Laboratory of Natural Medicines, Department of Natural Medicinal Chemistry, School of Traditional Chinese Pharmacy, China Pharmaceutical University, Nanjing 210009, China*

Yujin Wang − *State Key Laboratory of Natural Medicines, Department of Natural Medicinal Chemistry, School of Traditional Chinese Pharmacy, China Pharmaceutical University, Nanjing 210009, China*

Complete contact information is available at: https://pubs.acs.org/10.1021/acs.jmedchem.1c01099

Author Contributions

[§]K.W. and H.Z. contributed equally to this work.

Notes

The authors declare no competing financial interest.

■ ACKNOWLEDGMENTS

This research was supported by the National Natural Science Foundation of China (31870325 and 31500277), the Six-talent Peaks Project in Jiangsu Province (SWYY-071), and the "Double First Class" Subject Innovation Team Construction Project of China Pharmaceutical University (CPU2018GY12).

■ ABBREVIATIONS

Bcl-2, B-cell lymphoma-2; Bax, Bcl-2-associated X; Bad, Bcl-2 antagonist of cell death; CD31, platelet endothelial cell adhesion molecule-1; Cdc2, cell division cycle 2; Cyclin B1, cell division cyclin 25 homolog C; DAPI, 2-(4-amidinophenyl)-6-indolecarbamidine dihydrochloride; DCF-DA, 2′,7′-dichlorofluorescent yellow diacetate; DMSO, dimethylsulfoxide; EBI, *N*,*N*′-ethylenebis(iodoacetamide); FITC, fluorescein isothiocyanate; GAPDH, reduced glyceraldehyde-phosphate dehydrogenase; GTP, guanosine triphosphate; H&E, hematoxylin−eosin; JC-1, 5,5′,6,6′-tetrachloro-1,1′,3,3′-tetraethylimidacarbocyanine; MMP, mitochondrial membrane potential; MTAs, microtubule-targeting agents; MTT, 3-(4,5-dimethylthiazol-2-yl)-2,5-diphenyltetrazolium bromide; MVD, microvessel density; PARP, poly ADP-ribose polymerase; PI, propidium iodide; PTX, paclitaxel; iv, intravenous injection; ROS, reactive oxygen species; TUNEL, terminal deoxynucleotidyl transferase-mediated dUTP-biotin nick end labeling assay

https://doi.org/10.1021/acs.jmedchem.1c01099
J. Med. Chem. XXXX, XXX, XXX−XXX

REFERENCES

(1) Siegel, R. L.; Miller, K. D.; Jemal, A. Cancer statistics, 2019. *CA Cancer J. Clin.* **2019**, *69*, 7−34.

(2) Riggio, A. I.; Varley, K. E.; Welm, A. L. The lingering mysteries of metastatic recurrence in breast cancer. *Br. J. Cancer* **2021**, *124*, 13−26.

(3) Batran, R. Z.; Kassem, A. F.; Abbas, E. M.; Elseginy, S. A.; Mounier, M. M. Design, synthesis and molecular modeling of new 4-phenylcoumarin derivatives as tubulin polymerization inhibitors targeting MCF-7 breast cancer cells. *Bioorg. Med. Chem.* **2018**, *26*, 3474−3490.

(4) Qi, C.; Wang, X.; Shen, Z.; Chen, S.; Yu, H.; Williams, N.; Wang, G. Anti-mitotic chemotherapeutics promote apoptosis through TL1A-activated death receptor 3 in cancer cells. *Cell Res.* **2018**, *28*, 544−555.

(5) Jordan, M. A.; Wilson, L. Microtubules as a target for anticancer drugs. *Nat. Rev. Cancer* **2004**, *4*, 253−265.

(6) Mehlen, P.; Puisieux, A. Metastasis: a question of life or death. *Nat. Rev. Cancer* **2006**, *6*, 449−458.

(7) Dietrich, C.; Kaina, B. The aryl hydrocarbon receptor (AhR) in the regulation of cell−cell contact and tumor growth. *Carcinogenesis* **2010**, *31*, 1319−1328.

(8) Shan, A. Q.; Leng, L.; Li, J.; Luo, X. M.; Fan, Y. J.; Yang, Q. Y.; Xie, Q. H.; Chen, Y. S.; Ni, C. S.; Guo, L. M.; Tang, H.; Chen, X.; Tang, N. J. TCDD-induced antagonism of MEHP-mediated migration and invasion partly involves aryl hydrocarbon receptor in MCF7 breast cancer cells. *J. Hazard. Mater.* **2020**, *398*, No. 122869.

(9) Nebert, D. W.; Karp, C. L. Endogenous functions of the aryl hydrocarbon receptor (AHR): intersection of cytochrome P450 1 (CYP1)-metabolized eicosanoids and AHR biology. *J. Biol. Chem.* **2008**, *283*, 36061.

(10) Al-Dhfyan, A.; Alhoshani, A.; Korashy, H. M. Aryl hydrocarbon receptor/cytochrome P450 1A1 pathway mediates breast cancer stem cells expansion through PTEN inhibition and β-Catenin and Akt activation. *Mol. Cancer* **2017**, *16*, No. 1.

(11) Mulero-Navarro, S.; Pozo-Guisado, E.; Pérez-Mancera, P. A.; Alvarez-Barrientos, A.; Catalina-Fernández, I.; Hernández-Nieto, E.; Sáenz-Santamaria, J.; Martínez, N.; Rojas, J. M.; Sánchez-García, I.; Fernández-Salguero, P. M. Immortalized mouse mammary fibroblasts lacking dioxin receptor have impaired tumorigenicity in a subcutaneous mouse xenograft model. *J. Biol. Chem.* **2005**, *280*, 28731−28741.

(12) Afzal, O.; Kumar, S.; Haider, M. R.; Ali, M. R.; Kumar, R.; Jaggi, M.; Bawa, S. A review on anticancer potential of bioactive heterocycle quinoline. *Eur. J. Med. Chem.* **2015**, *97*, 871−910.

(13) Mahal, K.; Resch, M.; Ficner, R.; Schobert, R.; Biersack, B.; Mueller, T. Effects of the tumor-vasculature-disrupting agent verubulin and two heteroaryl analogues on cancer cells, endothelial cells, and blood vessels. *ChemMedChem* **2014**, *9*, 847−854.

(14) Zhou, Y. Y.; Yan, W.; Cao, D.; Shao, M. F.; Li, D.; Wang, F.; Yang, Z.; Chen, Y.; He, L. H.; Wang, T. J.; Shen, M. S.; Chen, L. J. Design, synthesis and biological evaluation of 4-anilinoquinoline derivatives as novel potent tubulin depolymerization agents. *Eur. J. Med. Chem.* **2017**, *138*, 1114−1125.

(15) Khelifi, I.; Naret, T.; Hamze, A.; Bignon, J.; Levaique, H.; Alvarez, M. C. G.; Dubois, J.; Provot, O.; Alami, M. N, N-bis-heteroaryl methylamines: Potent anti-mitotic and highly cytotoxic agents. *Eur. J. Med. Chem.* **2019**, *168*, 176−188.

(16) Fang, Z. Z.; Krausz, K. W.; Nagaoka, K.; Tanaka, N.; Gowda, K.; Amin, S. G.; Perdew, G. H.; Gonzalez, F. J. In vivo effects of the pure aryl hydrocarbon receptor antagonist GNF-351 after oral administration are limited to the gastrointestinal tract. *Br. J. Pharmacol.* **2014**, *171*, 1735−1746.

(17) Marinelli, L.; Martin-Gallausiaux, C.; Bourhis, J. M.; Béguet-Crespel, F.; Blottière, H. M.; Lapaque, N. Identification of the novel role of butyrate as AhR ligand in human intestinal epithelial cells. *Sci. Rep.* **2019**, *9*, No. 643.

(18) Pérez-Pérez, M. J.; Priego, E. M.; Bueno, O.; Martins, M. S.; Canela, M. D.; Liekens, S. Blocking blood flow to solid tumors by destabilizing tubulin: an approach to targeting tumor growth. *J. Med. Chem.* **2016**, *59*, 8685−8711.

(19) Fortin, S.; Lacroix, J.; Côté, M. F.; Moreau, E.; Petitclerc, É.; René, C. Quick and simple detection technique to assess the binding of antimicrotubule agents to the colchicine-binding site. *Biol. Proced. Online* **2010**, *12*, 113−117.

(20) Gaspari, R.; Prota, A. E.; Bargsten, K.; Cavalli, A.; Steinmetz, M. O. Structural basis of cis- and trans-combretastatin binding to tubulin. *Chem* **2017**, *2*, 102−113.

(21) Clarke, P. R.; Allan, L. A. Cell-cycle control in the face of damage-a matter of life or death. *Trends Cell Biol.* **2009**, *19*, 89−98.

(22) Buolamwini, J. K. Cell Cycle Molecular targets in novel anticancer drug discovery. *Curr. Pharm. Des.* **2000**, *6*, 379−392.

(23) Jordan, M. A.; Wilson, L. Microtubules and actin filaments: dynamic targets for cancer chemotherapy. *Curr. Opin. Cell Biol.* **1998**, *10*, 123−130.

(24) Vander Heiden, M. G.; Chandel, N. S.; Williamson, E. K.; Schumacker, P. T.; Thompson, C. B. Bcl-xL Regulates the membrane potential and volume homeostasis of mitochondria. *Cell* **1997**, *91*, 627−637.

(25) Circu, M. L.; Aw, T. Y. Reactive oxygen species, cellular redox systems, and apoptosis. *Free Radical Biol. Med.* **2010**, *48*, 749−762.

(26) Varga, I.; Hutóczki, G.; Petrás, M.; Scholtz, B.; Mikó, E.; Kenyeres, A.; Tóth, J.; Zahuczky, G.; Bognár, L.; Hanzély, Z.; Klekner, A. Expression of invasion-related extracellular matrix molecules in human glioblastoma versus intracerebral lung adenocarcinoma metastasis. *Cent. Eur. Neurosurg.* **2010**, *71*, 173−180.

https://doi.org/10.1021/acs.jmedchem.1c01099
J. Med. Chem. XXXX, XXX, XXX−XXX